

Azido-Functionalized Aromatic Phosphonate Esters in ^RPOSS-Cage-Supported Lanthanide Ion (Ln = La, Nd, Dy, Er) Coordination

Ingo Koehne, Miriam Gerstel, Clemens Bruhn, Johann P. Reithmaier, Mohamed Benyoucef, and Rudolf Pietschnig*

Cite This: *Inorg. Chem.* 2021, 60, 5297–5309

Read Online

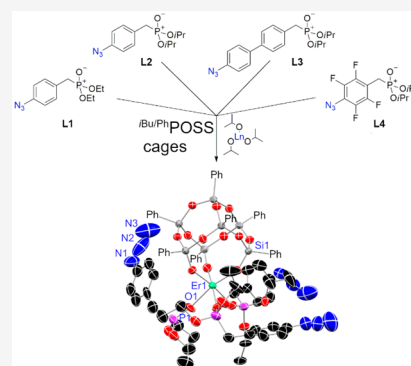
ACCESS |

Metrics & More

Article Recommendations

Supporting Information

ABSTRACT: Within this work, a modified preparation of diethyl 4-azidobenzylphosphonate (L1) is presented and the family of 4- or 4'-azido-substituted aromatic phosphonate esters is increased by three new ligand platforms: diisopropyl 4-azidobenzylphosphonate (L2), diisopropyl ((4'-azido-[1,1'-biphenyl]-4-yl)methyl)phosphonate (L3), and diisopropyl 4-azido-2,3,5,6-tetrafluorobenzylphosphonate (L4), which exhibit an anomalous splitting of the N₃ stretching vibrations. Subsequent coordination to the *in situ* generated ^RPOSS (polyhedral oligomeric silsesquioxane)-cage-supported lanthanide precursors [(Ln{^RPOSS})₂(THF)_{*m*}] (P1–P6) (Ln = La, Nd, Dy, Er; R = *i*Bu, Ph; *m* = 0, 1) yields complexes of the general formula [Ln{^RPOSS}(L1–L4)_{*n*}(S1)_{*x*}(THF)_{*m*}] (1–30) (*n* = 2, 3; *x* = 0, 1; *m* = 0–2) retaining the azide unit for future semiconductor surface immobilization. Because the latter compounds are mostly oils or viscous waxes, preliminary solution-state structure elucidations via DOSY-ECC-MW estimations have been carried out which are in accordance with ¹H NMR integral ratios as well as solid-state structures, where available. Moreover, the optical properties of the Nd, Dy, and Er derivatives of complexes 1–30 are examined in the visible and NIR spectral regions, where applicable.



INTRODUCTION

Lanthanide ions have already found widespread application in lighting, sensing, and display technologies, due to their outstanding photoluminescence properties.^{1–3} Moreover, lanthanides are promising candidates for implementation in quantum-based information storage on an atomic and molecular level. Recent progress in this field involves reading and manipulation of distinct spins^{4,5} and accessing atomic transitions for robust QuBits and magnetic data storage on single atoms.^{6,7}

In comparison to their carboxylic acid counterparts, the advantage of phosphonate esters arises from their lower vibrational frequencies, resulting in diminished nonemissive excited-state quenching and improved quantum yields.⁸ Our group has focused on these ligands in recent years, synthesizing several highly luminescent lanthanide-based MOFs^{9–11} as well as mono- and dimeric lanthanide complexes showing interesting splitting features in their NIR emission spectra.¹²

The compound class of organic azides has attracted attention of chemists all over the world since the characterization of phenyl azide by Griess over 155 years ago.¹³ Several members of the family are known to be labile and hence explosive and should be handled with care in the laboratory.¹⁴ Despite this property, organic azides have attracted broad industrial interest by proving to be versatile synthons in organic synthesis.^{15–17} Owing to their higher stability, aryl azides have found application, for example, as photoresistor

cross-linkers,¹⁸ in conducting polymers,¹⁹ and for light-induced polymer surface activation.^{15,20,21} Very recently, organic azides have been used for the modification of black phosphorus in a Staudinger-type reaction that is assumed to involve intermediate nitrenes.²² There are many approaches to aryl azide synthesis,^{14,15} and the most common way is to start from the corresponding aryl amine followed by a standard textbook diazotization reaction with NaNO₂ and subsequent treatment with NaN₃. A more elegant variation of this procedure under milder conditions involves *t*BuONO and TMSN₃.^{23,24} The metal-catalyzed azidation of organic molecules, especially Cu-mediated Ullmann-type coupling reactions of aryl halides,^{25,26} is an equally well established synthetic approach that has been reviewed recently by de Bruin et al.²⁷

To the best of our knowledge, there are only two other 4- or 4'-azido-substituted phosphonate esters known, which are summarized in Chart 1. Diethyl 4-azidobenzylphosphonate (L1) was used in a novel click-chemistry approach to flame-retardant polyurethanes,²⁸ while the ammonium salt of diethyl ((4-azidophenyl)difluoromethyl)phosphonate (A) was eval-

Received: January 27, 2021

Published: March 16, 2021

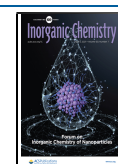
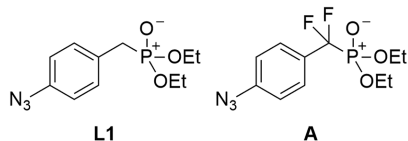


Chart 1. Known 4-Azido-Functionalized Phosphonate Ester Ligands L1 and A

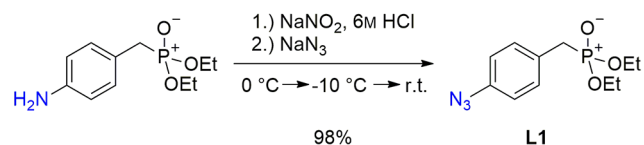


uated in terms of being a potent nonpeptidyl inhibitor of protein tyrosine phosphatase 1B.²⁹ Herein, we present a modified procedure for the preparation of **L1** as well as the synthesis of three new 4- or 4'-azido functionalized phosphonate ester ligands **L2**–**L4** comprising different aromatic backbones. In combination with our expertise in POSS (polyhedral oligomeric silsesquioxane)-cage chemistry,^{30–32} these ligands are then applied in ^RPOSS-cage-supported (R = *i*Bu, Ph) Ln³⁺ ion coordination to function as anchor groups for future immobilization of these complexes on (In/Ga)P semiconductor surfaces and subsequent evaluation of their potential as optically switchable isolated molecular quantum bits. In this context, an azido functionalization at the 4- or 4'-position of **L1**–**L4** is expected to be the most suitable to avoid steric congestion between a semiconductor surface and the rest of the POSS-cage-supported complexes. The rigid POSS-cage structure in combination with the phosphonate esters is assumed to enhance the excited-state lifetimes of the metal centers, paving the way for potential future molecular data storage and manipulation. For a comprehensive overview on POSS-cage as well as lanthanide POSS chemistry the reader is referred to the work of Edelmann and co-workers.^{33–36}

RESULTS AND DISCUSSION

Synthesis of Ligands L1–L4. Diethyl 4-azidobenzylphosphonate (**L1**) is prepared by starting from its 4-amino derivative via a modified procedure by Starikova and co-workers consisting of a standard textbook diazotization reaction and treatment with NaN₃.³⁷ An altered workup gives **L1** as an orange oil in a quantitative yield of 98% (Scheme 1).

Scheme 1. Synthesis of Ligand L1



Due to the lack of 4-amino derivatives, the synthesis of diisopropyl 4-azidobenzylphosphonate (**L2**) and diisopropyl ((4'-azido-[1,1'-biphenyl]-4-yl)methyl)phosphonate (**L3**) started from their 4-bromo derivatives **S1** and **S2**.¹² Following a modified protocol by Rodríguez et al., **L2** and **L3** are obtained in yields of 79% and 61%, respectively (Scheme 2, left).²⁸ The corresponding 4-amino-substituted side products **L2a** (10%) and **L3a** (12%) are obtained as well in this copper-mediated Ullmann-type coupling reaction. **L2a** and **L3a** again can be converted to the azides via a diazotization protocol and addition of NaN₃ or TMSN₃, increasing their theoretical yields to 89% and 73%, respectively. The underlying catalytic cycle is assumed to proceed via a Cu^I/Cu^{III} pair mediated oxidative addition–reductive elimination mechanism featuring a 4-fold-

coordinated Cu(III) species.^{25–27} Moreover, the formation of the amines **L2a** and **L3a** most likely proceeds via aryl anion radical intermediates and Cu(I) azide, as proposed in a comprehensive FT-IR study on copper-mediated one-pot reductive aminations of aryl halides by Monguchi et al.³⁸ The reactions had to be carried out in two steps (see the Experimental Section) due to the separation of elemental copper after 3 h of reaction time accompanied by a residual 25% of unreacted **S1**/**S2**. Therefore, an additional portion of the reagents was added again to target full turnover, and heating was continued for 3 h. Increasing the initial amounts of the reagents by ca. 25% also does not lead to full turnover but rather to the formation of more Cu(0). Interestingly, in the reaction starting from **S3**¹² the 4-protonated compound diisopropyl 2,3,5,6-tetrafluorobenzylphosphonate (**L4a**) is obtained in a yield of 66% instead of the 4-azido-substituted species. This may be a consequence of the strongly electron withdrawing (EWD) properties of the tetrafluorophenyl unit as in related cases.^{39,40} Moreover, these reaction conditions do not work either for the azidation of diisopropyl ((10-bromoanthracen-9-yl)methyl)phosphonate,¹² since only the starting material is quantitatively retrieved from the reaction mixture. Since no reaction takes place at all, it is most likely that the increased steric demand of the anthracene backbone is hampering an initial oxidative addition to the Cu(I) complex.

From vapor diffusion of pentanes into a saturated solution of **L3** in THF at –20 °C, only small needle-shaped crystals could be obtained that additionally suffered from decomposition by the X-ray irradiation after some time. X-ray data collection was additionally hampered by a phase transition of the crystals at 100 K, which required a measurement at an elevated temperature of 223 K. **L3** crystallizes in the monoclinic space group *P2₁/c* and does not show any π -stacking of the aromatic rings in the solid state (Figure 1, top; structural data are given in Table 1). Due to the poor data quality, no bond lengths or angles are discussed in the following. Crystals of **L3a** were obtained just as for **L3** but in good quality suitable for a proper SCXRD data collection. **L3a** crystallizes in the monoclinic space unit group *P2₁/n* containing one molecule in the asymmetric unit forming a three-dimensional hydrogen-bond network between adjacent molecules (Figure 1, bottom). In particular, the N–H...O_{P=O} distance of 2.10(2) Å and the N–H...O_{O–iPr} distance of 2.35(2) Å can be assigned to moderate and weak hydrogen-bond interactions, respectively.⁴¹ Moreover, the C₆ rings within the molecule are significantly twisted by 20.6(2)° with respect to each other despite forming a conjugated aromatic system. The phosphonate ester diisopropyl 4-azido-2,3,5,6-tetrafluorobenzylphosphonate (**L4**) is prepared in a four-step synthesis with a moderate overall yield of 30% starting from 2,3,4,5,6-pentafluorobenzaldehyde (Scheme 2, right). In a first step, an azido substituent is introduced at the *para* position of the starting material via a nucleophilic aromatic substitution (S_NAr), forming 4-azido-2,3,5,6-tetrafluorobenzaldehyde (**S4**).⁴² Next, reduction with NaBH₄ yields (4-amino-2,3,5,6-tetrafluorophenyl)methanol (**SS**), which is subsequently treated in an alcohol-based Michaelis–Arbuzov⁴³ reaction to give diisopropyl 4-amino-2,3,5,6-tetrafluorobenzylphosphonate (**S6**). In the last step, a diazotization is carried out using *t*BuONO followed by the addition of TMSN₃ to give the 4-azido-substituted target compound **L4**. During the reaction also a minor amount (ca. 8%) of the 4-protonated species **L4a** is formed that could not be removed by additional workup and column chromatog-

Scheme 2. Syntheses of Ligands L2 and L3 and Compounds L2a–L4a (Left) and of Compounds S4–S6 and L4a and Ligand L4 (Right)

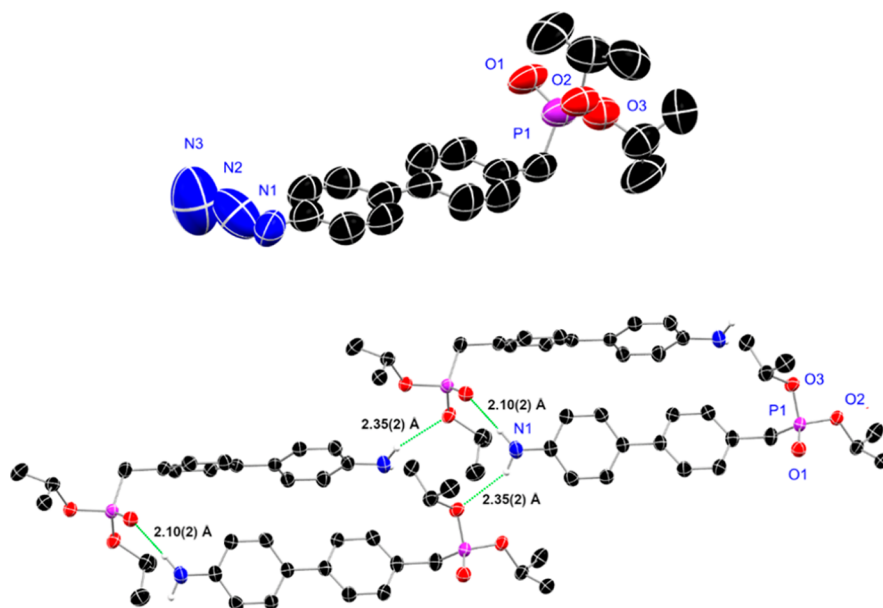
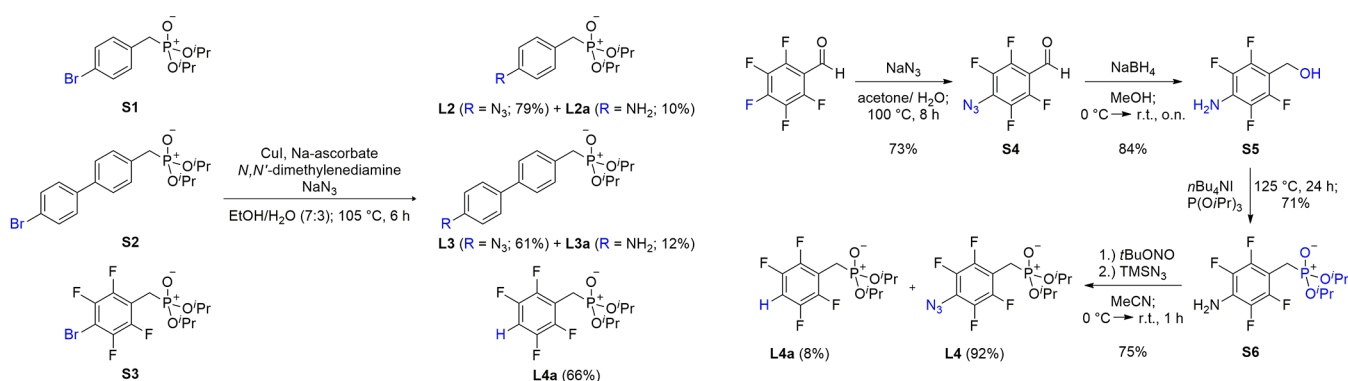


Figure 1. Molecular structures of L3 (top) and L3a (bottom) with the schematic 3D hydrogen-bond network. Anisotropic displacement parameters are depicted at the 50% probability level. With exception of the NH₂ groups, hydrogen atoms are omitted for clarity. Structural data are given in Table 1.

Table 1. Selected Bond Lengths (Å) and Angles (deg) of compounds L3a, S6, P5 as [Nd{^{Ph}POSS}(THF)₂]₂, 8, 31, and 32^a

compound	P=O	P–OR	M–O _{P=O}	M–O _{μ₁-OSi}	M–O _{μ₂-OSi}	M–O _{μ₃-OH}	O=P–C	M–O–P
L3a	1.467(2)	1.573(2)					113.1(11)	
S6	1.469(4)	1.565(4)					114.3(2)	
P5 as [Nd{ ^{Ph} POSS}(THF) ₂] ₂				2.228(6)	2.396(6)			
[Er{ ^{Ph} POSS}(L1) ₃] ₂ (8)	1.479(9)	1.560(9)	2.330(9)	2.165(9)			112.8(7)	152.7(7)
[Dy ₂ {T ₇ (O) ₃ }{T ₆ (OH) ₂ (O) ₂ }(μ ₃ -OH)(L2)] ₂ (31)	1.480(5)	1.565(6)	2.371(5)	2.315(5)	2.295(4)	2.374(4)	110.3(10)	158.0(4)
[Er ₂ {T ₇ (O) ₃ }{T ₆ (OH) ₂ (O) ₂ }(μ ₃ -OH)(L2)] ₂ (32)	1.471(5)	1.565(5)	2.344(5)	2.293(5)	2.277(4)	2.316(4)	111.6(8)	157.5(3)

^aAverage values are given for compounds with more than one molecule in the asymmetric unit or for more than one ligand of the same kind attached to a lanthanide ion.

raphy, leaving L4 as an orange oil in a purity of >92%. Crystals of S6 suitable for SCXRD experiments could be obtained via recrystallization from Et₂O/pentanes (2/1) at –20 °C.

The 4-amino phosphonate ester S6 crystallizes in the orthorhombic space group *Pna*2₁ containing four molecules in the unit cell (Figure 2). In contrast to L3a a two-dimensional hydrogen-bond network is exclusively formed between the NH₂ groups and neighboring P=O phosphonate

moieties consisting of weak to moderate interactions with N–H···O_{P=O} distances in a range of 2.09(2)–2.25(2) Å.

A comparison of L1–L4 and L2a–L4a shows that ³¹P NMR shifts in a range from 19.6 to 26.3 ppm are recorded for the phosphonate ester moieties (Table 2). Within the row, L1 exhibits the most deshielded and L4 the most shielded resonance due to the highest number of EWD substituents at the ligand backbone. In contrast, the compound ((4-azidophenyl)difluoromethyl)phosphonate (A) shows a

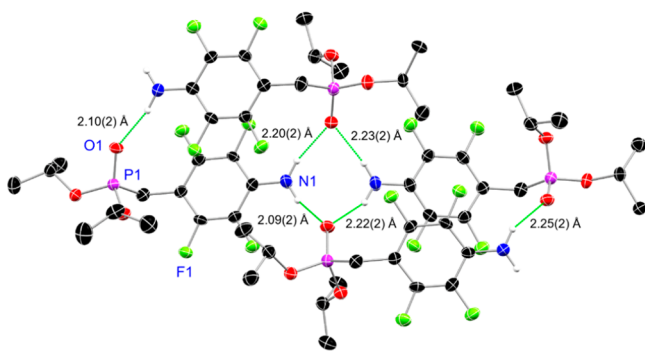


Figure 2. Molecular structure of diisopropyl 4-amino-2,3,5,6-tetrafluorobenzylphosphonate (**S6**) with the schematic 2D hydrogen-bond network. Anisotropic displacement parameters are depicted at the 50% probability level. With the exception of NH_2 groups, hydrogen atoms are omitted for clarity. Structural data are given in Table 1.

Table 2. ^{31}P NMR Shifts (ppm) and Selected IR Vibrations (cm^{-1}) of Ligands **L1–L4** and Compounds **A** and **L2a–L4a**

	^{31}P NMR	$\nu_{\text{as}}(\text{N}_3)$	$\nu_{\text{s}}(\text{N}_3)$	$\nu(\text{NH}_2)$
L1	26.3	2111	1391, 1381	
L2	24.1	2112	1384, 1374	
L3	24.3	2122, 2092	1385, 1374	
L4	19.6	2168, 2119	1386, 1376	
A ²⁹	3.9	2149		
L2a	24.6			3341 (ν_{as}), 3234 (ν_{s})
L3a	24.7			3335 (ν_{as}), 3239 (ν_{s})
L4a	19.7			

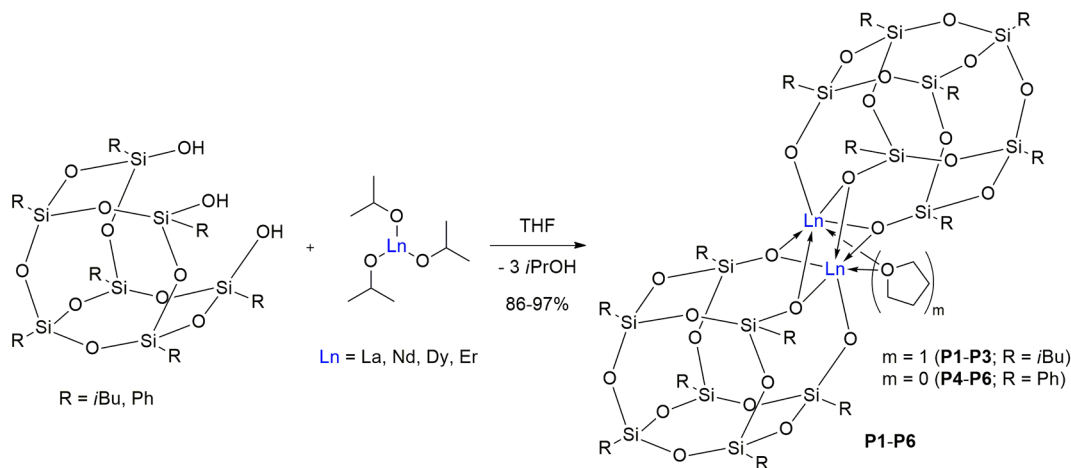
strongly shielded signal at 3.9 ppm caused by the EWD effect of the fluorinated methylene bridge adjacent to the phosphorus. The ^{31}P resonances of compounds **L2a–L4a** all experience a slight deep-field shift in comparison to their 4-azido-substituted counterparts. The asymmetric and symmetric stretches of the N_3 substituent are typically found around 2100 and 1400 cm^{-1} , respectively.⁴⁴ As expected for **L1** and **L2**, one intense band for the asymmetric vibration is recorded at 2111 and 2112 cm^{-1} , respectively. In contrast, the $\nu_{\text{as}}(\text{N}_3)$ vibrational mode is anomalously split into two bands of medium intensity at 2122 and 2092 cm^{-1} for **L3** and of strongly deviating intensity at 2168 and 2119 cm^{-1} for **L4** (see

the Supporting Information). This phenomenon can be ascribed to Fermi interactions with combination tones including the symmetric N_3 or C–N stretching mode and other low-lying frequencies.⁴⁵ Nonetheless, in comparison to **A**, which exhibits a $\nu_{\text{as}}(\text{N}_3)$ band at 2149 cm^{-1} , all the asymmetric vibrations are significantly red shifted. A similar splitting of the symmetric N_3 stretch around 1374–1391 cm^{-1} is observed in all four phosphonates that is most blue shifted in **L1**. Contrasting trends are found for the 4-amino-substituted species **L2a** and **L3a**. In comparison to **L2a**, the $\nu_{\text{as}}(\text{NH}_2)$ vibration in **L3a** is red-shifted while the $\nu_{\text{s}}(\text{NH}_2)$ band is slightly blue shifted.

^RPOSS Cage-based Lanthanide Precursors **P1–P6**

Lanthanide precursors **P1–P6** with the general solution-state structure $[(\text{Ln}\{\text{R}^{\text{POSS}}\})_2(\text{THF})_m]$ ($\text{Ln} = \text{La, Nd, Er}$; $\text{R} = i\text{Bu, Ph}$; $m = 0, 1$) (see the section on DOSY) are obtained in a concerted deprotonation–metalation reaction between a ^RPOSS cage ($\text{R} = i\text{Bu, Ph}$) and the corresponding lanthanide(III) isopropoxides in dry THF (Scheme 3). **P1–P6** are obtained as white, blue, or pink solids in isolable yields of 86–97%. Crystallization from different solvents afforded unique coordination motifs in the solid state. From a solution of **P3** in dry pentanes, a tetrameric structure of the form $[\text{Er}_4\{\text{iBu}^{\text{POSS}}\}_2\{\text{iBu}^{\text{POSS}}_{\text{Si-OH}}\}_2(\mu_4\text{-O})]$ is obtained at -20°C featuring a μ_4 -oxo ligand and partially protonated POSS cages (Figure 3). The cages at the Er1 ions are still trianionic, while those at the Er2 ions are now dianionic ligands, offering two Si-O^- groups as well as a Si-OH moiety. In general, the Er^{3+} ions are μ_2 -bridged by two Si-O^- moieties of each POSS cage, while the third donor site shows an exclusive coordination to either Er1 (Si-O^-) or Er2 (Si-OH), giving in total a 6-fold, distorted-octahedral oxygen coordination. Because water is formed in the synthesis of POSS cages, the incorporated water molecule most likely originates from traces of water in the POSS cage starting material. The tetramer *en bloc* forms a tetrahedrally shaped structure with the μ_4 -oxo ligand residing at the center of the Er_4 plane. Owing to poor data quality, no bond lengths or angles are considered in the following. The present coordination motif is in close agreement with a very similar structure by Shen and co-workers.⁴⁶ Here, a Nd^{3+} tetramer of the form $[(\text{Nd}\{\text{iBu}^{\text{POSS}}\})_4\text{NaCl}]$ was obtained that shows a similar coordination motif by formally hosting a NaCl molecule. In

Scheme 3. Syntheses of Lanthanide Precursors **P1–P6** Showing Their Estimated Solution-State Structure



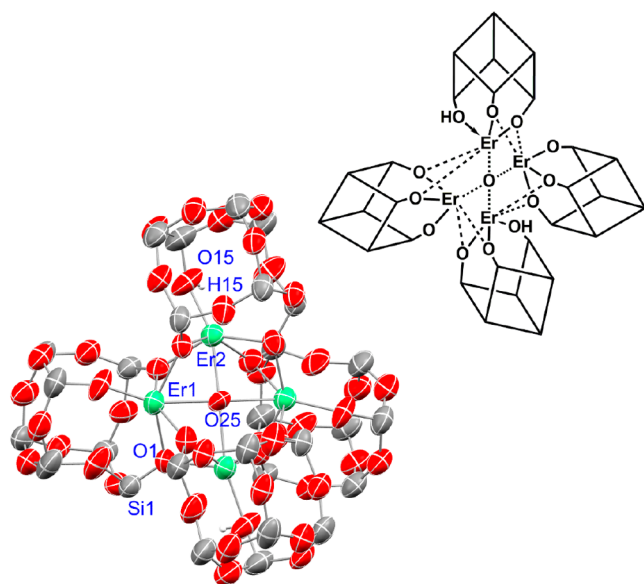


Figure 3. Molecular structure of $[\text{Er}_4\{\text{tBuPOSS}\}_2\{\text{tBuPOSS}_{\text{Si-OH}}\}_2(\mu_4\text{-O})]$ from a solution of **P3** in dry pentanes at $-20\text{ }^\circ\text{C}$. Anisotropic displacement parameters are depicted at the 30% probability level. The *t*Bu substituents are omitted for clarity. A schematic drawing is given to clarify the binding situation. Symmetry code: (#1) $-x + 3/2, y, -z + 3/2$.

this complex the O^{2-} is replaced by a Cl^- anion while two Na^+ cations are residing above and below the Nd_4 plane that each exhibit an occupancy of 1/2. The absence of OH stretching modes above 3000 cm^{-1} in the IR spectrum of $[\text{Er}_4\{\text{tBuPOSS}\}_2\{\text{tBuPOSS}_{\text{Si-OH}}\}_2(\mu_4\text{-O})]$ (see the [Supporting Information](#)) indicates intramolecular hydrogen bonding of the two Si–OH groups with the silanolate units in proximity.⁴¹ For comparison, other rarely found lanthanide tetramers such as $\text{Na}_6\{\text{[PhSiO}_2\text{]}_8\text{Ln}_4(\mu_4\text{-O})[\text{O}_2\text{SiPh}]_8\}\cdot 10\text{EtOH}\cdot 8\text{H}_2\text{O}$ ($\text{Ln} = \text{Nd, Gd, Dy}$) containing a central $\mu_4\text{-O}^{2-}$ ligand have been obtained from their anhydrous lanthanide chlorides and eight-membered sodium phenylsiloxanates.⁴⁷ The hydrogen positions are not fully resolved in these structures, but due to charge compensation of the hexaanion by six sodium ions, the presence of a O^{2-} dianion residing at the Ln_4 plane is most likely.

From vapor diffusion of pentanes into a concentrated solution of **P5** in THF a dimeric solid-state structure of the form $[\text{Nd}\{\text{PhPOSS}\}(\text{THF})_2]_2$ is obtained at $-20\text{ }^\circ\text{C}$. This species crystallizes in the monoclinic space group $P2_1/c$ containing half of the dimer in the asymmetric unit ([Figure 4](#)). The other half is generated by an inversion center. Each Nd^{3+} cation exhibits a 7-fold distorted-pentagonal-bipyramidal oxygen coordination, but in this case only one of the three Si–O[−] moieties of each POSS cage shows a μ_2 -bridging mode between the metal centers. To complete the coordination sphere, each metal ion is additionally coordinated by two THF donor molecules.

L1–L4-Based ^RPOSS-lanthanide Complexes 1–30. The **L1–L4**- and ^RPOSS-cage-supported complexes **1–30** of the general formula $[\text{Ln}\{\text{RPOSS}\}(\text{L1–L4})_n(\text{S1})_x(\text{THF})_m]$ ($\text{Ln} = \text{La, Nd, Dy, Er}$; $\text{R} = \text{iBu, Ph}$; $n = 2, 3$; $x = 0, 1$; $m = 0–2$) are obtained from *in situ* generated lanthanide POSS cage complexes and subsequent addition of one of the 4-azido-substituted phosphonate esters in yields of 73–88% ([Scheme 4](#)). In the case of **L2**, a 2:1 mixture of **L2** and its 4-bromo-

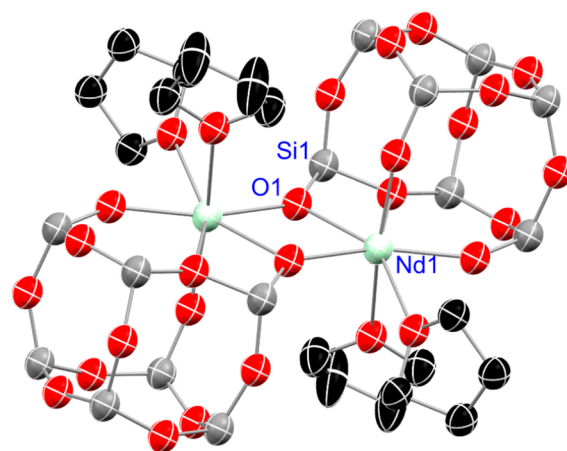


Figure 4. Molecular structure of $[\text{Nd}\{\text{PhPOSS}\}(\text{THF})_2]_2$ from vapor diffusion of pentanes into a saturated solution of **P5** in THF. Anisotropic displacement parameters are depicted at the 50% probability level. Hydrogens and phenyl substituents are omitted for clarity. Structural data are given in [Table 1](#). Symmetry code: (#1) $-x + 1, -y + 1, -z$.

substituted species **S1** was prepared to provide enough phosphonate ligand for subsequent complexation. In case of the more sterically demanding **L3**, reactions with addition of only 2 equiv were performed because ¹H-DOSY-MW estimation experiments of previous reactions with 3 equiv suggested the coordination of only two **L3** ligands to the La^{3+} ions in solution (see section on [DOSY](#)). Moreover, no reaction with $\text{Dy}(\text{OiPr})_3$ has been performed for **L3** and the corresponding ^{iBu/Ph}POSS cages. A preliminary solution-state structure elucidation was also carried out via ¹H-DOSY NMR spectroscopy for the La^{3+} species **1, 5, 9, 13, 17, 20, 23, and 27** (see section on [DOSY](#)). Except for the complexes $[\text{Ln}\{\text{PhPOSS}\}(\text{L3})_2(\text{THF})_2]$ (**20–22**) ($\text{Ln} = \text{La, Nd, Er}$) that are obtained as beige solids, brownish-orange viscous oils or sticky waxes are obtained for compounds **1–19** and **23–30**. Only in a few cases do these oils or waxes start to solidify after some time under argon, and only for the complex $[\text{Er}\{\text{PhPOSS}\}(\text{L1})_3]$ (**8**) were crystals suitable for SCXRD experiments obtained. **8** crystallizes in the monoclinic space group $P2_1$ containing one molecule in the asymmetric unit ([Figure 5](#)). Despite being formally tridentate ligands, the phosphonate esters exclusively coordinate via their P=O oxygen atom to the central Er^{3+} cation. In combination with the tridentate coordination by the ^{Ph}POSS cage, a 6-fold distorted-octahedral coordination is established.

The ³¹P NMR resonances of the La^{3+} complexes **1, 5, 9, 13, 17, 20, 23, 27** are found in a range of 19.5–25.5 ppm ([Table 3](#)). Only in the case of ligand **L1** (26.3 ppm) are significant high-field shifts of the ³¹P NMR signals by 0.8 ppm in **1** and even 2.5 ppm in **5** observed upon metal ion coordination. For phosphonate esters **L2–L4**, less pronounced high-field shifts of 0.1–0.2 ppm are detected upon complex formation. Again, a splitting of the asymmetric and symmetric azide stretches is observed for the **L3**- and **L4**-based complexes and for the symmetric stretch in the **L2**-based and ^{Ph}POSS-supported complexes. In comparison to the free ligands, the $\nu_{\text{as}}(\text{N}_3)$ vibrations generally experience a slight shift to higher wavenumbers while the $\nu_{\text{s}}(\text{N}_3)$ modes are mostly unaffected by the lanthanide ion coordination. The ²⁹Si NMR resonances of the protonated POSS cages can be found with a ratio of

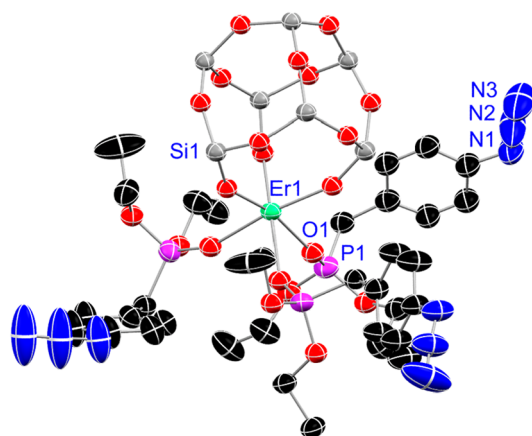
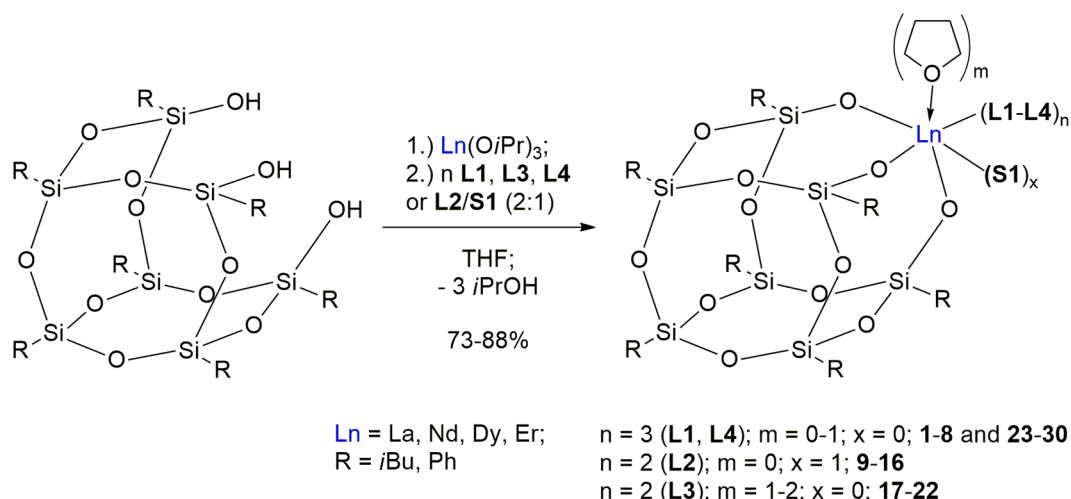
Scheme 4. Syntheses of L1–L4-Based ^RPOSS-lanthanide Complexes 1–30

Figure 5. Molecular structure of $[\text{Er}\{\text{PhPOSS}\}(\text{L1})_3]$ (**8**). Anisotropic displacement parameters are depicted at the 50% probability level. Hydrogens and phenyl substituents are omitted for clarity. Structural data are given in Table 1.

3:1:3 at -59.1 , -67.5 , and -68.8 ppm and at -69.1 , -77.6 , and -78.6 ppm for the *i*Bu- and Ph-substituted derivatives, respectively. However, the ^{29}Si spectra of the La^{3+} complexes reveal the presence of five to seven signals for the seven cage silicon atoms within this range that partially fall close together. In turn, this indicates a loss of symmetry within the cages of the obtained complexes, resulting in the acquisition of an increased number of silicon resonances. This symmetry loss accompanied by dynamic processes is also reflected by broadened and fanned-out signals of the *i*Bu and Ph groups in their ^1H and ^{13}C NMR spectra.

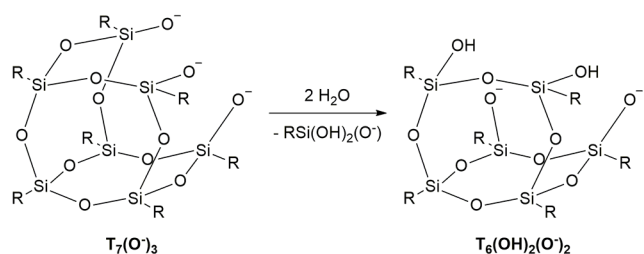
A transfer of complexes **1–30** from Schlenk vessels to vials under ambient conditions results in the formation of a few crystals at the upper inside of these vials in some cases and after some time. In the cases where crystals suitable for SCXRD experiments were obtained, the solid-state structures reveal their corresponding predecessors $[\text{Ln}\{\text{iBuPOSS}\}(\text{L2})_2(\text{S1})]$ ($\text{Ln} = \text{Dy}$ (**11**), Er (**12**)) to have suffered from partial $\text{T}_7(\text{O}^-)_3$ cage rearrangement induced by a reaction with airborne water with cleavage of one of the cage silicon edges (Scheme 5). Now, the formed $\text{T}_6(\text{OH})_2(\text{O}^-)_2$ cages are dianionic tetradentate ligands offering two $\text{Si}-\text{O}^-$ as well as

Table 3. ^{31}P NMR Shifts (ppm) and N_3 Vibrations (cm^{-1}) of Complexes 1–30

complex	^{31}P	$\nu_{\text{as}}(\text{N}_3)$	$\nu_{\text{s}}(\text{N}_3)$
$[\text{La}\{\text{iBuPOSS}\}(\text{L1})_3]$ (1)	25.5	2113	1401
$[\text{Nd}\{\text{iBuPOSS}\}(\text{L1})_3]$ (2)		2113	1401
$[\text{Dy}\{\text{iBuPOSS}\}(\text{L1})_3]$ (3)		2114	1401
$[\text{Er}\{\text{iBuPOSS}\}(\text{L1})_3]$ (4)		2113	1401
$[\text{La}\{\text{PhPOSS}\}(\text{L1})_3]$ (5)	23.8	2112	1393
$[\text{Nd}\{\text{PhPOSS}\}(\text{L1})_3]$ (6)		2112	1394
$[\text{Dy}\{\text{PhPOSS}\}(\text{L1})_3]$ (7)		2112	1395
$[\text{Er}\{\text{PhPOSS}\}(\text{L1})_3]$ (8)		2111	1394
$[\text{La}\{\text{iBuPOSS}\}(\text{L2})_2(\text{S1})]$ (9)	23.9, 25.3	2114	1385
$[\text{Nd}\{\text{iBuPOSS}\}(\text{L2})_2(\text{S1})]$ (10)		2113	1384
$[\text{Dy}\{\text{iBuPOSS}\}(\text{L2})_2(\text{S1})]$ (11)		2114	1385
$[\text{Er}\{\text{iBuPOSS}\}(\text{L2})_2(\text{S1})]$ (12)		2113	1385
$[\text{La}\{\text{PhPOSS}\}(\text{L2})_2(\text{S1})]$ (13)	24.2, 25.5	2113	1386, 1375
$[\text{Nd}\{\text{PhPOSS}\}(\text{L2})_2(\text{S1})]$ (14)		2113	1386, 1376
$[\text{Dy}\{\text{PhPOSS}\}(\text{L2})_2(\text{S1})]$ (15)		2113	1386, 1376
$[\text{Er}\{\text{PhPOSS}\}(\text{L2})_2(\text{S1})]$ (16)		2113	1386, 1376
$[\text{La}\{\text{iBuPOSS}\}(\text{L3})_2(\text{THF})]$ (17)	24.1	2122, 2092	1384, 1365
$[\text{Nd}\{\text{iBuPOSS}\}(\text{L3})_2(\text{THF})]$ (18)		2124, 2095	
$[\text{Er}\{\text{iBuPOSS}\}(\text{L3})_2(\text{THF})]$ (19)		2123, 2093	1385, 1376
$[\text{La}\{\text{PhPOSS}\}(\text{L3})_2(\text{THF})_2]$ (20)	24.2	2119, 2092	1386, 1376
$[\text{Nd}\{\text{PhPOSS}\}(\text{L3})_2(\text{THF})_2]$ (21)		2120, 2092	1386, 1376
$[\text{Er}\{\text{PhPOSS}\}(\text{L3})_2(\text{THF})_2]$ (22)		2118, 2092	1386, 1376
$[\text{La}\{\text{iBuPOSS}\}(\text{L4})_3]$ (23)	19.5	2170, 2119	1386, 1377
$[\text{Nd}\{\text{iBuPOSS}\}(\text{L4})_3]$ (24)		2174, 2119	1386, 1377
$[\text{Dy}\{\text{iBuPOSS}\}(\text{L4})_3]$ (25)		2168, 2119	1386, 1378
$[\text{Er}\{\text{iBuPOSS}\}(\text{L4})_3]$ (26)		2171, 2119	1386, 1378
$[\text{La}\{\text{PhPOSS}\}(\text{L4})_3(\text{THF})]$ (27)	19.6	2173, 2119	1387, 1377
$[\text{Nd}\{\text{PhPOSS}\}(\text{L4})_3(\text{THF})]$ (28)		2172, 2119	1387, 1377
$[\text{Dy}\{\text{PhPOSS}\}(\text{L4})_3(\text{THF})]$ (29)		2171, 2119	1387, 1377
$[\text{Er}\{\text{PhPOSS}\}(\text{L4})_3(\text{THF})]$ (30)		2171, 2118	1387, 1377

two $\text{Si}-\text{OH}$ moieties. The obtained isostructural tetrameric lanthanide complexes of the form $[\text{Ln}_2\{\text{T}_7(\text{O}^-)_3\}-\{\text{T}_6(\text{OH})_2(\text{O}^-)_2\}(\mu_3-\text{OH})(\text{L2})]_2$ ($\text{Ln} = \text{Dy}$ (**31**), Er (**32**)) crystallize in the monoclinic space group $P2_1/n$ (Figure 6). On the one hand, these compounds exhibit two terminal, 6-fold-coordinated Ln^{3+} cations ($\text{Ln}1$) where each is exclusively coordinated by a $\text{T}_7(\text{O}^-)_3$ cage, by the two $\text{T}_6(\text{OH})_2(\text{O}^-)_2$

Scheme 5. Schematic Water-Induced Cleavage of a Silicon Edge from the Trianionic $T_7(O^-)_3$ Cages under Formation of Dianionic $T_6(OH)_2(O^-)_2$ Cages



cages, and by a μ_3 -bridging hydroxo ligand (O27). On the other hand, there are two lateral Ln^{3+} ions (Ln_2) that each show a 7-fold coordination made up by one of the $T_6(OH)_2(O^-)_2$ cages, an oxygen of a 4-azido phosphonate ester ligand, and two μ_3 -hydroxo ligands. In general, the $Si-O^-$ moieties of the $T_6(OH)_2(O^-)_2$ cages show a μ_2 -bridging motif to the terminal and lateral metal ions while the $Si-OH$ groups each display a single coordination to one of the lateral lanthanide ions. The formed intramolecular $OH\cdots O$ hydrogen bond distances of 1.62(2) Å (H23) and 1.68(2) Å (H15) are on the edge of being strong interactions, while an $OH\cdots O$ distance of 2.18(2) Å for H27 is at the junction of weak electrostatic and dispersion force interactions.⁴¹ Related tetranuclear lanthanide complexes comprising μ_3 -capping

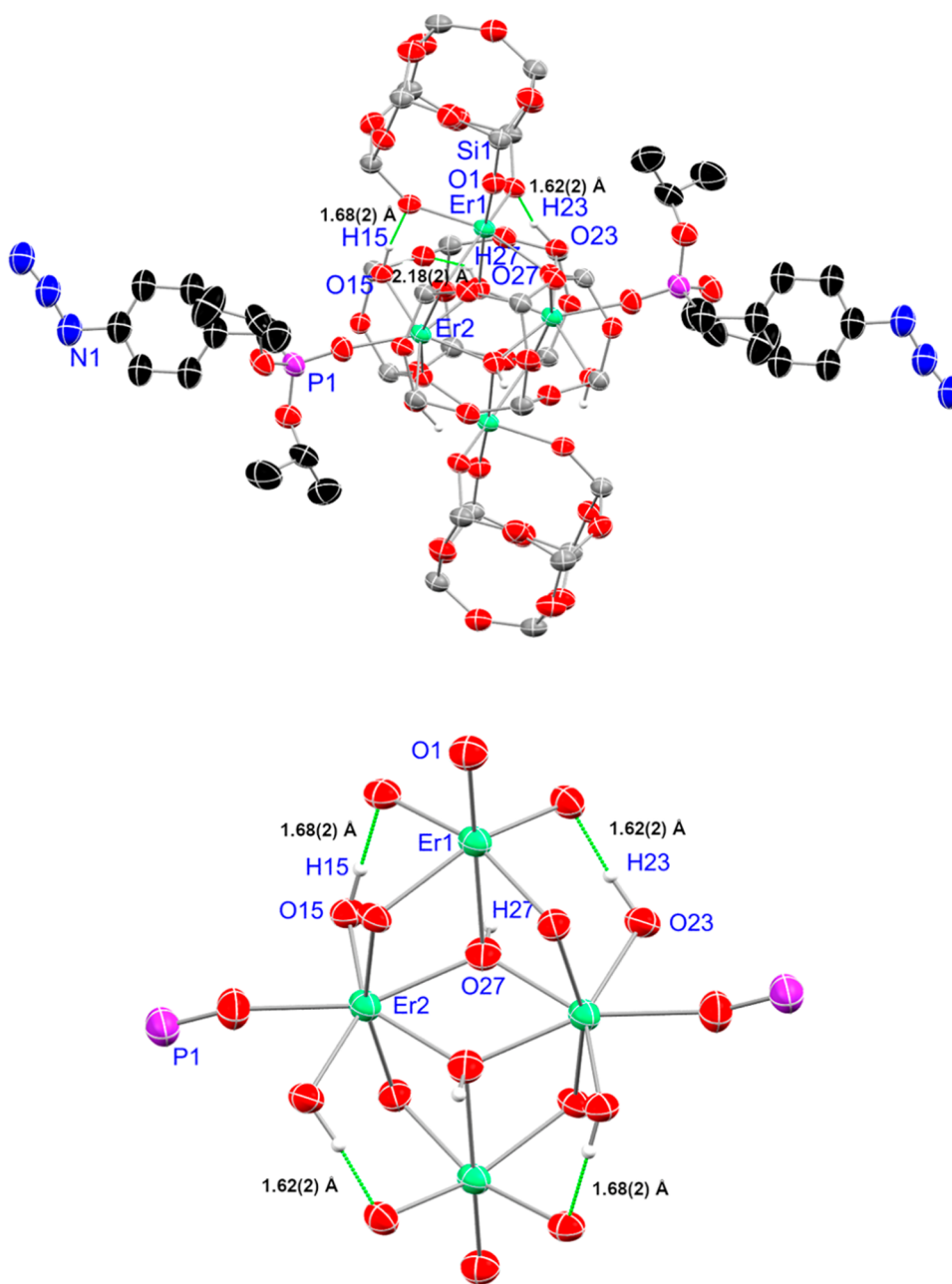


Figure 6. Molecular structure of $[Er_2\{T_7(O)_3\}\{T_6(OH)_2(O)_2\}[\mu_3-OH](L_2)]_2$ (32) (top) and a drawing of the first coordination sphere of the Er^{3+} ions to clarify the binding situation (bottom). Anisotropic displacement parameters are depicted at the 50% probability level. Except for OH groups, hydrogens and *i*Bu substituents are omitted for clarity. Structural data for 31 and 32 are given in Table 1. Symm. code: #1 $-x+1, -y+1, -z+1$.

Table 4. ^1H -DOSY-ECC-MW Estimation of P1, P4, 1, 5, 9, 13, 17, 20, 23, and 27 in C_6D_6 or CDCl_3 at rt

complex	MW _{theo} (g/mol)	MW _{DSE} (g/mol) (MW _{dif} (%))	MW _{merge} (g/mol) (MW _{dif} (%))
$[(\text{La}\{\text{t}^{\text{Bu}}\text{POSS}\})_2(\text{THF})]$ (P1)	1927	1858 (4)	2305 (−16)
$[(\text{La}\{\text{Ph}\text{POSS}\})_2]$ (P4)	2135	1837 (16)	2276 (−6)
$[\text{La}\{\text{t}^{\text{Bu}}\text{POSS}\}(\text{L1})_3]$ (1)	1735	1497 (16)	1822 (−5)
$[\text{La}\{\text{Ph}\text{POSS}\}(\text{L1})_3]$ (5)	1875	1555 (21)	1898 (−1)
$[\text{La}\{\text{t}^{\text{Bu}}\text{POSS}\}(\text{L2})_2(\text{S1})]$ (9)	1857	1365 (36)	1667 (13)
$[\text{La}\{\text{Ph}\text{POSS}\}(\text{L2})_2(\text{S1})]$ (13)	1997	1386 (44)	1675 (19)
$[\text{La}\{\text{t}^{\text{Bu}}\text{POSS}\}(\text{L3})_2(\text{THF})]$ (17)	1746	1508 (16)	1836 (−5)
$[\text{La}\{\text{Ph}\text{POSS}\}(\text{L3})_2(\text{THF})_2]$ (20)	1958	1950 (0)	2428 (−19)
$[\text{La}\{\text{t}^{\text{Bu}}\text{POSS}\}(\text{L4})_3]$ (23)	2035	1526 (33)	1860 (9)
$[\text{La}\{\text{Ph}\text{POSS}\}(\text{L4})_3(\text{THF})]$ (27)	2247	1549 (45)	1903 (18)

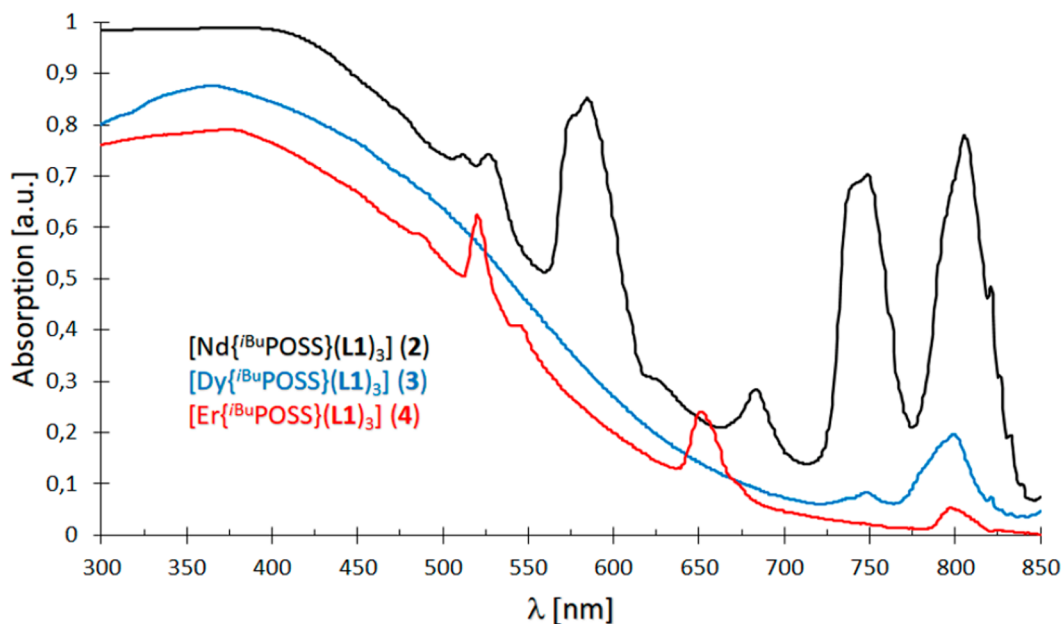


Figure 7. Exemplary absorption spectra of complexes 2 (black), 3 (blue), and 4 (red) at rt exhibiting typically sharp Nd^{3+} , Dy^{3+} , and Er^{3+} absorption bands.

hydroxo ligands contain cubane-like $[\text{Ln}_4(\mu_3\text{-OH})_4]^{8+}$ cluster cores and comparable $\text{M}-\text{O}_{\mu_3\text{-OH}}$ distances.⁴⁸ Moreover, a comparison with the tetrameric solid-state structure of $[\text{Er}_4\{\text{t}^{\text{Bu}}\text{POSS}\}_2\{\text{t}^{\text{Bu}}\text{POSS}_{\text{Si-OH}}\}_2(\mu_4\text{-O})]$ obtained from precursor P3 indicates this structure as reflecting the intermediate state of a reaction with water on the way to partially decomposed POSS cages as found in compounds 31 and 32.

An evaluation of selected bond lengths shows the $\text{P}=\text{O}$ distances of the free phosphonate esters as becoming slightly elongated upon lanthanide ion coordination. This is in accordance with a red shift of the $\text{P}=\text{O}$ vibration of the free ligands L1–L3 in combination with the $\text{t}^{\text{Bu}}\text{POSS}$ -cage-supported complexes. Interestingly, in combination with the PhPOSS -cage-based lanthanides, the $\text{P}=\text{O}$ vibration in L1–L3 experiences a blue shift. Only in the case of L4 does the $\text{P}=\text{O}$ stretch experience an expected red shift for both, the $\text{t}^{\text{Bu}}\text{POSS}$ - and the PhPOSS -cage-supported lanthanide compounds. The $\text{M}-\text{O}_{\text{P}=\text{O}}$ distances in 8, 31 and 32 are in a range from 2.330(9) to 2.371(5) Å and decrease from Dy^{3+} to the smaller Er^{3+} cation, which is also observed for the $\text{M}-\text{O}_{\mu_3\text{-OH}}$ bond lengths. A similar trend can be derived for the corresponding $\text{M}-\text{O}_{\mu_2\text{-OSi}}$ distances, which decrease from 2.396(6) Å in $[\text{Nd}\{\text{Ph}\text{POSS}\}(\text{THF})_2]_2$ over 2.295(4) Å in 31 to 2.277(4) Å

in 32, which is in accordance with the successively decreasing effective ionic radii of the lanthanide ions: Nd^{3+} (98 pm) > Dy^{3+} (91 pm) > Er^{3+} (89 pm).⁴⁹ The considered $\text{O}=\text{P}-\text{C}$ angles experience a slight shortening from an average of $113.7(11)^\circ$ in the free phosphonate esters to an average of $111.6(10)^\circ$ in the complexed ligands. The shortest $\text{M}-\text{O}-\text{P}$ angles with an average of $152.7(7)^\circ$ are found in the monomeric complex $[\text{Er}\{\text{Ph}\text{POSS}\}(\text{L1})_3]$ (8), while this angle decreases in the tetrameric compounds from $158.0(4)^\circ$ in the Dy^{3+} species 31 to $157.5(3)^\circ$ in the Er^{3+} species 32.

^1H -DOSY-ECC-MW Estimation Study. A preliminary solution-state structure elucidation of the La^{3+} complexes P1, P4, 1, 5, 9, 13, 17, 20, 23, and 27 was performed via a ^1H -DOSY external calibration curve (ECC) molecular weight (MW) estimation.^{50–53} Previous studies showed that for most organometallic compounds the dissipated spheres and ellipsoids (DSE) calibration curve is most suitable for an accurate estimation.⁵⁴ Hence, only values from the DSE and, for comparison, from the merged calibration curve are considered (Table 4). Although this method is only strongly reliable for molecules with a weight of up to 600 g/mol, a previous study has shown that good results are still obtained for aggregates up to 1000 g/mol.⁵⁵ However, the obtained results have to be considered carefully and shall rather serve as

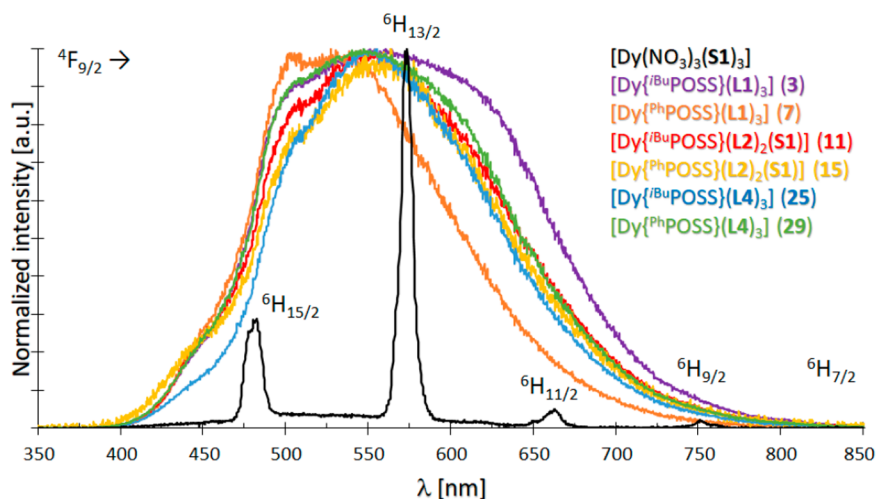


Figure 8. Superimposed room-temperature μ -PL emission spectra ($\lambda_{\text{exc}} = 355$ nm) of Dy^{3+} complexes $[\text{Dy}(\text{NO}_3)_3(\text{S1})_3]$ (black), 3 (purple), 7 (orange), 11 (red), 15 (yellow), 25 (blue), and 29 (green). The spectra are normalized to their emission band maximum.

guidance in combination with other spectroscopic methods (for detailed DOSY data, see the [Supporting Information](#)). As expected, with the exception of **P1** and complex **20**, more or less strongly deviating DSE values are obtained for the assumed La^{3+} aggregates with molecular weights of around 2000 g/mol. In contrast, good to fair values are still estimated from the merged calibration curve for all considered complexes showing a deviation (MW_{dif}) from their theoretically calculated molecular weights (MW_{theo}) between 1 and 19%. The estimated MW values suggest the presence of dimeric species for the precursors **P1** and **P4** and monomeric species for complexes **1**, **5**, **9**, **13**, **17**, **20**, **23**, and **27** in solution that most likely carry one or two additional THF donor molecules in some cases. Thus, in accordance with and supported by ^1H NMR integral ratios, the solid-state structures obtained for complex **P5** and $[\text{Er}\{\text{PhPOSS}\}(\text{L1})_3]$ (**8**), as well as the data from elemental analysis, the molecular formulas given in [Table 4](#) are derived for the considered La^{3+} complexes and their Nd, Dy, and Er congeners. Despite the fact that the crystal structure obtained from **P5** in THF shows coordinating THF donor molecules, it is most likely that in the $^{\text{PhPOSS}}$ -supported precursors **P4**–**P6** there are no additional THF molecules attached to the metal ions in solution because complex- and THF-related signals show significantly deviating diffusion coefficients in the DOSY spectrum of **P4** (see the [Supporting Information](#)). Moreover, the signals are sharp, so that a fast exchange between attached and detached THF molecules can most likely be excluded.

Photoluminescence (PL) Properties. Absorption Properties of Nd^{3+} , Dy^{3+} , and Er^{3+} Complexes. The absorption spectra of the Nd^{3+} , Dy^{3+} and Er^{3+} complexes presented herein basically look the same, exhibiting the anticipated metal-centered absorption bands in a range of 300–850 nm of the Nd^{3+} ($\lambda_{\text{abs,max}} = 586$ nm), Dy^{3+} ($\lambda_{\text{abs,max}} = 802$ nm), and Er^{3+} ($\lambda_{\text{abs,max}} = 521$ nm) cations, respectively. Some exemplary spectra of complexes $[\text{Nd}\{\text{tBuPOSS}\}(\text{L1})_3]$ (**2**) (black), $[\text{Dy}\{\text{tBuPOSS}\}(\text{L1})_3]$ (**3**) (blue) and $[\text{Er}\{\text{tBuPOSS}\}(\text{L1})_3]$ (**4**) (red) are summarized in [Figure 7](#), showing all three lanthanide ions sharing an absorption band at around 800 nm. Additionally, the recorded spectra all show a strong and broad absorption of the azido-substituted phosphonate ester ligands in a range between 300 and 700 nm that slowly decreases with

increasing wavelength but still covers some of the metal-centered absorptions.

Emission Properties of the Dy^{3+} Complexes. In the range between 350 and 850 nm, Dy^{3+} -centered emissions from the $^4\text{F}_{9/2}$ level can be detected around 480 ($\rightarrow ^6\text{H}_{15/2}$), 570 ($\rightarrow ^6\text{H}_{13/2}$), 660 ($\rightarrow ^6\text{H}_{11/2}$), 750 ($\rightarrow ^6\text{H}_{9/2}$), and 840 nm ($\rightarrow ^6\text{H}_{7/2}$), like those shown for the phosphonate ester supported model complex $[\text{Dy}(\text{NO}_3)_3(\text{S1})_3]$ ([Figure 8](#), black).¹² However, unless the signals are amplified by e.g. ligand to metal charge transfer (LMCT), all complexes are expected to show no or only very weak metal-centered emissions due to Laporte-forbidden 4f–4f transitions. To recognize these weak emissions, spectra were recorded with a microphotoluminescence (μ -PL) spectrometer. An excitation of the weakly fluorescent Dy^{3+} complexes **3**, **7**, **11**, **15**, **25**, and **29** at 355 nm results in the detection of only one broad emission band in the region of the aforementioned energy transitions, simultaneously excluding the presence of LMCT processes in these systems ([Figure 8](#), colored spectra). This band covers the metal-centered emissions and can be ascribed to the phosphonate ester ligands (see the [Supporting Information](#)).

Emission Properties of the Nd^{3+} and Er^{3+} Complexes. In addition to the detection of ligand emission upon UV irradiation, the metal-centered emissions were also investigated by using excitation laser wavelengths of 750 nm (Nd^{3+}) and 800 nm (Er^{3+}), respectively. Due to the relatively weak absorption band of Er^{3+} at around 800 nm ([Figure 7](#)), the characteristic emission at about 1550 nm⁵⁶ was not observed. However, μ -PL spectra could be recorded for **L1**–**L4**- and $^{\text{RPOSS}}$ -cage-supported Nd^{3+} complexes **2**, **6**, **10**, **14**, **18**, **21**, **24**, **28** and **P5**, where three emission bands centered at about 900, 1060, and 1330 nm are observed that correspond to the $^4\text{F}_{3/2} \rightarrow ^4\text{I}_{9/2}$, $^4\text{F}_{3/2} \rightarrow ^4\text{I}_{11/2}$ and $^4\text{F}_{3/2} \rightarrow ^4\text{I}_{13/2}$ transitions, respectively ([Figure 9](#)). The μ -PL spectra are similar to those that we have recently reported in a study on exclusively phosphonate ester supported Nd^{3+} complexes.¹²

In comparison, the **L1**–**L4**- and $^{\text{RPOSS}}$ -cage-supported Nd^{3+} complexes presented in this work show relatively low emission intensities with some noise. The weak PL emission might be explained by the rigid structure of the POSS cage stabilizing the metal-centered excited states. As we have

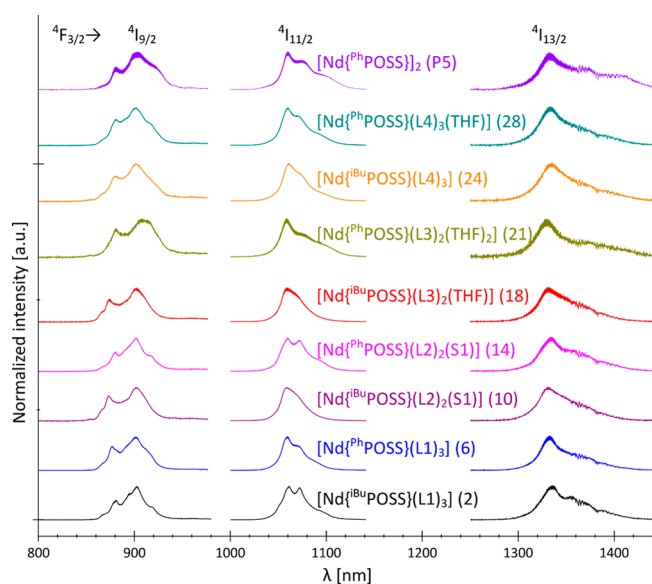


Figure 9. Stacked room temperature μ -PL emission spectra ($\lambda_{\text{exc}} = 750$ nm) of Nd^{3+} complexes **2** (black), **6** (blue), **10** (magenta), **14** (pink), **18** (red), **21** (green), **24** (orange), **28** (cyan), and **P5** (purple). There are three emission bands in the NIR, corresponding to the ${}^4\text{F}_{3/2} \rightarrow {}^4\text{I}_{9/2}$, ${}^4\text{F}_{3/2} \rightarrow {}^4\text{I}_{11/2}$ and ${}^4\text{F}_{3/2} \rightarrow {}^4\text{I}_{13/2}$ transitions. The spectra are normalized to the emission band maximum of each recorded transition.

already reported, the exclusively phosphonate ester supported Nd^{3+} complexes exhibit a splitting feature in their emission spectra.¹² For the ${}^4\text{F}_{3/2} \rightarrow {}^4\text{I}_{9/2}$ transition, the most pronounced splitting is observed of about 22 nm. For the ${}^4\text{F}_{3/2} \rightarrow {}^4\text{I}_{11/2}$ and ${}^4\text{F}_{3/2} \rightarrow {}^4\text{I}_{13/2}$ transitions, splittings of 28 and 47 nm were recorded, respectively. The splitting was tentatively assigned to electrostatic ligand–metal orbital interactions which influence the electrons of the Nd^{3+} ion, as was previously reported for a similar splitting feature observed for Eu^{3+} clusters.⁵⁷ In particular, the splitting was attributed to an electrostatic interaction of Eu^{3+} -centered f orbitals and O-centered orbitals of adjacent oxo ligands.

CONCLUSIONS

A modified synthetic protocol of diethyl 4-azidobenzylphosphonate (**L1**) as well as the preparation of the three novel azide-functionalized ligand platforms diisopropyl 4-azidobenzylphosphonate (**L2**), diisopropyl ((4'-azido-[1,1'-biphenyl]-4-yl)-methyl)phosphonate (**L3**) and diisopropyl 4-azido-2,3,5,6-tetrafluorobenzylphosphonate (**L4**) is presented. All ligands exhibit an anomalous splitting of their symmetric and/or asymmetric azide stretching modes that can be ascribed to Fermi interactions with combination tones including the symmetric N_3 or C–N stretching mode and other low-lying frequencies.⁴⁵ From reactions of R^{POSS} cages with lanthanide isopropoxides lanthanide precursor complexes with the general solution-state structure $[(\text{Ln}\{\text{R}^{\text{POSS}}\})_2(\text{THF})_m]$ (**P1–P6**) ($\text{Ln} = \text{La}, \text{Nd}, \text{Er}$; $\text{R} = i\text{Bu}, \text{Ph}$; $m = 0, 1$) are obtained that show unique coordination motifs in the solid state depending on their crystallization conditions in donating or nondonating solvents. A complex of the form $[\text{Er}_4\{\text{R}^{\text{POSS}}\}_2\{\text{R}^{\text{POSS}}\}_{\text{Si-OH}}\}_2(\mu_4\text{-O})]$ is obtained from a solution of **P3** in dry pentanes at -20 °C. The incorporation of a water molecule results in the coordination of a μ_4 -oxo ligand in the Er_4 plane with two of the four POSS cages being

partially protonated, thus providing two anionic Si-O^- and one neutral Si-OH donor site. From a combination of *in situ* generated POSS-supported lanthanide precursors with ligands **L1–L4**, complexes of the general formula $[\text{Ln}\{\text{R}^{\text{POSS}}\}(\text{L1–L4})_n(\text{S1})_x(\text{THF})_m]$ (**1–30**) ($\text{Ln} = \text{La}, \text{Nd}, \text{Dy}, \text{Er}$; $n = 2, 3$; $x = 0, 1$; $m = 0–2$) are formed. The derived complex formulas are supported by recorded NMR data, X-ray structures, elemental analyses, and a preliminary ${}^1\text{H}$ -DOSY-ECC-MW estimation study. The coordinated phosphonate esters show an unusual splitting of the symmetric and/or asymmetric azide stretching modes. Handling of compounds **1–30** under ambient conditions results in a slow decomposition of some of these complexes induced by airborne water. For the compounds $[\text{Ln}\{\text{R}^{\text{POSS}}\}(\text{L2})_2(\text{S1})]$ ($\text{Ln} = \text{Dy}$ (**11**), Er (**12**)), solid-state structures of the general formula $[\text{Ln}_2\{\text{T}_7(\text{O})_3\}\{\text{T}_6(\text{OH})_2(\text{O})_2\}(\mu_3\text{-OH})(\text{L2})_2]$ ($\text{Ln} = \text{Dy}$ (**31**), Er (**32**)) are obtained under ambient conditions exhibiting partial $\text{T}_7(\text{O}^-)_3$ cage decomposition with the formation of μ_3 -OH bridged tetramers. Moreover, absorption and emission spectra of the Nd^{3+} , Dy^{3+} , and Er^{3+} complexes are recorded to explore their potential as optically switchable isolated molecular quantum bits. In addition to ligand-centered emission, the microphotoluminescence (μ -PL) spectra of the Nd^{3+} compounds **2**, **6**, **10**, **14**, **18**, **21**, **24**, **28**, and **P5** show three metal-centered emission bands ascribed to ${}^4\text{F}_{3/2} \rightarrow {}^4\text{I}_{9/2}$, ${}^4\text{F}_{3/2} \rightarrow {}^4\text{I}_{11/2}$, and ${}^4\text{F}_{3/2} \rightarrow {}^4\text{I}_{13/2}$ transitions, which are similar to those recently reported for exclusively phosphonate ester based Nd^{3+} model complexes.¹² The μ -PL spectra of the Dy^{3+} complexes **3**, **7**, **11**, **15**, **25**, and **29** only exhibit broad ligand emission in a range from 400 to 800 nm that completely covers possibly detectable metal-centered emissions in this region. Unexpectedly, no metal-centered emission at around 1550 nm⁵⁶ could be detected for one of the present Er^{3+} complexes.

EXPERIMENTAL SECTION

General Information. All manipulations involving air- and moisture-sensitive compounds were carried out under an argon atmosphere using Schlenk techniques or handled in an argon glovebox. Solvents were dried over Na or K metal or Na/K alloy and were used freshly distilled. Starting materials were purchased commercially and were used as received, unless stated otherwise. $\text{Dy}(\text{O}i\text{Pr})_3$ ⁵⁸ and **S1–S3** were prepared according to literature procedures.¹² Filtering of moisture-sensitive compounds was carried out with self-made filter cannulas assembled from Whatman fiberglass filters (GF/B, 25 mm), which were applied with Teflon tape to Teflon cannulas. Flash chromatography was performed with an Interchim PuriFlash XS 520Plus device using PF-30SHP-F0020 and -F0040 columns (CV = column volumes). For TLC, precoated Macherey-Nagel Alugram Xtra SIL G/UV₂₅₄ plates were used. NMR experiments were performed with Varian 400 and 500 MHz spectrometers, and spectra were processed with MestReNova (v11.0.4-18998, Mestrelab Research S.L.). ${}^1\text{H}$ and ${}^{13}\text{C}$ NMR spectra were referenced relative to TMS using the residual solvent signals as internal standards.⁵⁹ DOSY-NMR experiments were recorded on a Varian 400 MHz spectrometer. Sample spinning was deactivated during the measurements, and the temperature was set and controlled at 298 K. All DOSY experiments were performed using the Dbppste pulse sequence.⁶⁰ DOSY transformation and processing was carried out with MestReNova (v11.0.4-18998, Mestrelab Research S.L.). Molecular weight estimation was carried out with the software (v1.3) provided by Bachmann.⁵² IR spectra were recorded with a Bruker diamond probe ATR IR spectrometer. Elemental analyses were performed using a HEKAtech Euro EA-CHNS elemental analyzer. For analyses, samples were prepared in tin cups with V_2O_5 as an additive to ensure complete combustion. ESI mass spectra were recorded on a Finnigan LCQDeca (ThermoQuest) or a MicroTOF

(Bruker Daltonics) device. GC-MS mass spectra were obtained using a Thermo Scientific DSQ II device. Absorption spectra were acquired with a Hamamatsu C11347 device in the range of 250–850 nm. Two different setups were used for room-temperature μ -PL experiments. The Dy complexes were excited at 355 nm, and the PL signal was guided through a glass fiber to an OceanOptics USB2000+ spectrometer. For Nd complexes ($\lambda_{\text{exc}} = 750$ nm), the laser was focused on the complexes by a microscope objective (NA = 0.7) to a spot size of ~ 1 μm . The same objective was used to collect the emission from the complexes. The luminescence was spectrally filtered by a 0.75 m focal length spectrometer equipped with a liquid N₂ cooled InGaAs detector. The μ -PL spectra were taken with a laser excitation power of 50 mW.

Crystallographic Details. X-ray diffraction experiments were performed with either a STOE IPDS 2 diffractometer with an image plate (\varnothing 34 cm) using a Mo-GENIX source ($\lambda = 0.71073$ nm) or a STOE StadiVari instrument with DECTRIS PILATUS 200 K using a Cu-GENIX source ($\lambda = 1.54186$ nm). All structures were solved using direct methods (SHELXT)⁶¹ and refined against F^2 using the full-matrix least-squares methods of SHELXL⁶² within the SHELXLE GUI⁶³ or with OLEX2.⁶⁴ Additional programs used for structural analysis included Mercury⁶⁵ and Platon.⁶⁶ CCDC 2050303–2050310 contain the supplementary crystallographic data for this paper.

■ ASSOCIATED CONTENT

SI Supporting Information

The Supporting Information is available free of charge at <https://pubs.acs.org/doi/10.1021/acs.inorgchem.1c00266>.

Experimental procedures, NMR, DOSY, IR, and PL spectra, and detailed DOSY and X-ray data (PDF)

Accession Codes

CCDC 2050303–2050310 contain the supplementary crystallographic data for this paper. These data can be obtained free of charge via www.ccdc.cam.ac.uk/data_request/cif, or by emailing data_request@ccdc.cam.ac.uk, or by contacting The Cambridge Crystallographic Data Centre, 12 Union Road, Cambridge CB2 1EZ, UK; fax: +44 1223 336033.

■ AUTHOR INFORMATION

Corresponding Author

Rudolf Pietschnig – Institute of Chemistry and Center for Interdisciplinary Nanostructure Science and Technology (CINSA^T), University of Kassel, 34132 Kassel, Germany; orcid.org/0000-0003-0551-3633; Email: pietschnig@uni-kassel.de; www.uni-kassel.de/go/hym

Authors

Ingo Koehne – Institute of Chemistry and Center for Interdisciplinary Nanostructure Science and Technology (CINSA^T), University of Kassel, 34132 Kassel, Germany; orcid.org/0000-0001-7294-5095

Miriam Gerstel – Institute of Nanostructure Technologies and Analytics (INA) and CINSA^T, University of Kassel, 34132 Kassel, Germany

Clemens Bruhn – Institute of Chemistry and Center for Interdisciplinary Nanostructure Science and Technology (CINSA^T), University of Kassel, 34132 Kassel, Germany

Johann P. Reithmaier – Institute of Nanostructure Technologies and Analytics (INA) and CINSA^T, University of Kassel, 34132 Kassel, Germany

Mohamed Benyoucef – Institute of Nanostructure Technologies and Analytics (INA) and CINSA^T, University of Kassel, 34132 Kassel, Germany

Complete contact information is available at:

<https://pubs.acs.org/10.1021/acs.inorgchem.1c00266>

Author Contributions

The manuscript was written through contributions of all authors. All authors have given approval to the final version of the manuscript.

Notes

The authors declare no competing financial interest.

■ ACKNOWLEDGMENTS

The federal state of Hesse, Germany, is kindly acknowledged for financial support of the SMolBits project within the LOEWE program.

■ DEDICATION

Dedicated to Prof. Dr. Wolfgang Kaim on the occasion of his 70th birthday.

■ REFERENCES

- (1) Guillou, O.; Daiguebonne, C.; Calvez, G.; Bernot, K. A Long Journey in Lanthanide Chemistry: From Fundamental Crystallography Studies to Commercial Anticounterfeiting Taggants. *Acc. Chem. Res.* **2016**, *49* (5), 844–856.
- (2) Bünzli, J.-C. Europium in the limelight. *Nat. Chem.* **2010**, *2* (8), 696–696.
- (3) Samson, B.; Carter, A.; Tankala, K. Rare-earth fibres power up. *Nat. Photonics* **2011**, *5* (8), 466–467.
- (4) Vincent, R.; Klyatskaya, S.; Ruben, M.; Wernsdorfer, W.; Balestro, F. Electronic read-out of a single nuclear spin using a molecular spin transistor. *Nature* **2012**, *488* (7411), 357–360.
- (5) Thiele, S.; Balestro, F.; Ballou, R.; Klyatskaya, S.; Ruben, M.; Wernsdorfer, W. Electrically driven nuclear spin resonance in single-molecule magnets. *Science* **2014**, *344* (6188), 1135–1138.
- (6) Donati, F.; Rusponi, S.; Stepanow, S.; Wäckerlin, C.; Singha, A.; Persichetti, L.; Baltic, R.; Diller, K.; Patthey, F.; Fernandes, E.; Dreiser, J.; Šljivančanin, Ž.; Kummer, K.; Nistor, C.; Gambardella, P.; Brune, H. Magnetic remanence in single atoms. *Science* **2016**, *352* (6283), 318–321.
- (7) Natterer, F. D.; Yang, K.; Paul, W.; Willke, P.; Choi, T.; Greber, T.; Heinrich, A. J.; Lutz, C. P. Reading and writing single-atom magnets. *Nature* **2017**, *543* (7644), 226–228.
- (8) Hasegawa, Y.; Kimura, Y.; Murakoshi, K.; Wada, Y.; Kim, J.-H.; Nakashima, N.; Yamanaka, T.; Yanagida, S. Enhanced Emission of Deuterated Tris(hexafluoroacetylacetonato)-neodymium(III) Complex in Solution by Suppression of Radiationless Transition via Vibrational Excitation. *J. Phys. Chem.* **1996**, *100* (24), 10201–10205.
- (9) Krekić, K.; Klintuch, D.; Pietschnig, R. Facile access to efficiently luminescent Ln³⁺ phosphonic ester coordination polymers (Ln = Eu, Tb, Dy). *Chem. Commun.* **2017**, *53* (80), 11076–11079.
- (10) Krekić, K.; Käkel, E.; Klintuch, D.; Bloß, D.; Pietschnig, R. Coordination Polymers based on the Neutral Ditopic Ligand (C₆H₄PO(OCH₃)₂)₂ Involving some f-Block Elements. *Z. Anorg. Allg. Chem.* **2018**, *644* (3), 149–154.
- (11) Krekić, K.; Klintuch, D.; Lescop, C.; Calvez, G.; Pietschnig, R. Structural and Luminescence Properties of Anthracene- and Biphenyl-Based Lanthanide Bisphosphonate Ester Coordination Polymers. *Inorg. Chem.* **2019**, *58* (1), 382–390.
- (12) Koehne, I.; Lik, A.; Gerstel, M.; Bruhn, C.; Reithmaier, J. P.; Benyoucef, M.; Pietschnig, R. Functionalised phosphonate ester supported lanthanide (Ln = La, Nd, Dy, Er) complexes. *Dalton Trans.* **2020**, *49* (46), 16683–16692.
- (13) Griess, P. Über eine neue Klasse organischer Verbindungen, in denen Wasserstoff durch Stickstoff vertreten ist. *Justus Liebigs Ann. Chem.* **1866**, *137* (1), 39–91.
- (14) Scriven, E. F. V.; Turnbull, K. Azides: their preparation and synthetic uses. *Chem. Rev.* **1988**, *88* (2), 297–368.

- (15) Bräse, S.; Gil, C.; Knepper, K.; Zimmermann, V. Organic Azides: An Exploding Diversity of a Unique Class of Compounds. *Angew. Chem., Int. Ed.* **2005**, *44* (33), 5188–5240.
- (16) Huang, D.; Yan, G. Recent Advances in Reactions of Azides. *Adv. Synth. Catal.* **2017**, *359* (10), 1600–1619.
- (17) Banert, K. The Chemistry of Unusually Functionalized Azides. *Synthesis* **2016**, *48* (15), 2361–2375.
- (18) Cai, S. X.; Glenn, D. J.; Kanskar, M.; Wybourne, M. N.; Keana, J. F. W. Development of Highly Efficient Deep-UV and Electron Beam Mediated Cross-Linkers: Synthesis and Photolysis of Bis-(perfluorophenyl) Azides. *Chem. Mater.* **1994**, *6* (10), 1822–1829.
- (19) Meijer, E. W.; Nijhuis, S.; Van Vroonhoven, F. C. B. M. Poly-1,2-azepines by the photopolymerization of phenyl azides. Precursors for conducting polymer films. *J. Am. Chem. Soc.* **1988**, *110* (21), 7209–7210.
- (20) Cai, S. X.; Glenn, D. J.; Keana, J. F. W. Toward the development of radiolabeled fluorophenyl azide-based photolabeling reagents: synthesis and photolysis of iodinated 4-azidoperfluorobenzoates and 4-azido-3,5,6-trifluorobenzoates. *J. Org. Chem.* **1992**, *57* (4), 1299–1304.
- (21) Nahar, P.; Wali, N. M.; Gandhi, R. P. Light-Induced Activation of an Inert Surface for Covalent Immobilization of a Protein Ligand. *Anal. Biochem.* **2001**, *294* (2), 148–153.
- (22) Walz Mitra, K.; Chang, C. H.; Hanrahan, M. P.; Yang, J.; Tofan, D.; Holden, W. M.; Govind, N.; Seidler, G.; Rossini, A. J.; Velian, A. Surface Functionalization of Black Phosphorus with Nitrenes: Identification of P = N Bonds Using Isotopic Labeling. *Angew. Chem., Int. Ed.* **2020**, DOI: 10.1002/anie.202016033.
- (23) Barral, K.; Moorhouse, A. D.; Moses, J. E. Efficient Conversion of Aromatic Amines into Azides: A One-Pot Synthesis of Triazole Linkages. *Org. Lett.* **2007**, *9* (9), 1809–1811.
- (24) Zanato, C.; Cascio, M. G.; Lazzari, P.; Pertwee, R.; Testa, A.; Zanda, M. Tricyclic Fused Pyrazoles with a ‘Click’ 1,2,3-Triazole Substituent in Position 3 Are Nanomolar CB1 Receptor Ligands. *Synthesis* **2015**, *47* (06), 817–826.
- (25) Ma, D.; Cai, Q. Copper/Amino Acid Catalyzed Cross-Couplings of Aryl and Vinyl Halides with Nucleophiles. *Acc. Chem. Res.* **2008**, *41* (11), 1450–1460.
- (26) Hajjipour, A. R.; Karimzadeh, M.; Ghorbani, S. Selective Azidation of Aryl Halides to Aryl Azides Promoted by Proline and CuFeO₂. *Synlett* **2014**, *25* (20), 2903–2907.
- (27) Goswami, M.; de Bruin, B. Metal-Catalysed Azidation of Organic Molecules. *Eur. J. Org. Chem.* **2017**, *2017* (8), 1152–1176.
- (28) Borreguero, A. M.; Sharma, P.; Spiteri, C.; Velencoso, M. M.; Carmona, M. S.; Moses, J. E.; Rodriguez, J. F. A novel click-chemistry approach to flame retardant polyurethanes. *React. Funct. Polym.* **2013**, *73* (9), 1207–1212.
- (29) Taylor, S. D.; Kotoris, C. C.; Dinaut, A. N.; Wang, Q.; Ramachandran, C.; Huang, Z. Potent non-peptidyl inhibitors of protein tyrosine phosphatase 1B. *Bioorg. Med. Chem.* **1998**, *6* (9), 1457–1468.
- (30) Spirk, S.; Nieger, M.; Belaj, F.; Pietschnig, R. Formation and hydrogen bonding of a novel POSS-trisilanol. *Dalton Trans.* **2009**, No. 1, 163–167.
- (31) Hurkes, N.; Bruhn, C.; Belaj, F.; Pietschnig, R. Silanetriols as Powerful Starting Materials for Selective Condensation to Bulky POSS Cages. *Organometallics* **2014**, *33* (24), 7299–7306.
- (32) Kahr, J.; Belaj, F.; Pietschnig, R. Preparation and Molecular Structure of a Cyclopentyl-Substituted Cage Hexasilsesquioxane T₆ (T = cyclopentyl-SiO_{1.5}) Starting from the Corresponding Silanetriol. *Inorganics* **2017**, *5* (4), 66.
- (33) Lorenz, V.; Fischer, A.; Gießmann, S.; Gilje, J. W.; Gun'ko, Y.; Jacob, K.; Edelmann, F. T. Disiloxanediolates and polyhedral metasilsesquioxanes of the early transition metals and f-elements. *Coord. Chem. Rev.* **2000**, *206–207*, 321–368.
- (34) Lorenz, V.; Edelmann, F. T. Metasilsesquioxanes. *Adv. Organomet. Chem.* **2005**, *53*, 101–153.
- (35) Lorenz, V.; Edelmann, A.; Gießmann, S.; Hrib, C. G.; Blaurock, S.; Edelmann, F. T. Disiloxanediolates and Metasilsesquioxanes of the Rare Earth Elements. *Z. Anorg. Allg. Chem.* **2010**, *636* (12), 2172–2191.
- (36) Gießmann, S.; Lorenz, V.; Liebing, P.; Hilfert, L.; Fischer, A.; Edelmann, F. T. Synthesis and structural study of new metasilsesquioxanes of potassium and uranium. *Dalton Trans.* **2017**, *46* (8), 2415–2419.
- (37) Ponomarev, I. I.; Zharinova, M. Y.; Klemenkova, Z. S.; Petrovskii, P. V.; Starikova, Z. A. Synthesis of N-(2-hydroxyphenyl)-1,8-naphthalimide and its derivatization at the hydroxy group. *Russ. Chem. Bull.* **2011**, *60* (3), 512.
- (38) Maejima, T.; Ueda, M.; Nakano, J.; Sawama, Y.; Monguchi, Y.; Sajiki, H. Mechanism Study of Copper-Mediated One-Pot Reductive Amination of Aryl Halides Using Trimethylsilyl Azide. *J. Org. Chem.* **2013**, *78* (18), 8980–8985.
- (39) Orthaber, A.; Seidel, C.; Belaj, F.; Albering, J. H.; Pietschnig, R.; Ruschewitz, U. Optimized Synthesis of Tetrafluoroterephthalic Acid: A Versatile Linking Ligand for the Construction of New Coordination Polymers and Metal-Organic Frameworks. *Inorg. Chem.* **2010**, *49* (20), 9350–9357.
- (40) Orthaber, A.; Belaj, F.; Pietschnig, R. A fluoroaryl substituent with spectator function: Reactivity and structures of cyclic and acyclic HF₄C₆-substituted phosphanes. *J. Organomet. Chem.* **2010**, *695* (7), 974–980.
- (41) Steiner, T. The Hydrogen Bond in the Solid State. *Angew. Chem., Int. Ed.* **2002**, *41* (1), 48–76.
- (42) Keana, J. F. W.; Cai, S. X. New reagents for photoaffinity labeling: synthesis and photolysis of functionalized perfluorophenyl azides. *J. Org. Chem.* **1990**, *55* (11), 3640–3647.
- (43) Ma, X.; Xu, Q.; Li, H.; Su, C.; Yu, L.; Zhang, X.; Cao, H.; Han, L.-B. Alcohol-based Michaelis-Arbuzov reaction: an efficient and environmentally-benign method for C-P(O) bond formation. *Green Chem.* **2018**, *20* (15), 3408–3413.
- (44) Diana, E.; Gatterer, K.; Kettle, S. F. A. The vibrational spectroscopy of the coordinated azide anion; a theoretical study. *Phys. Chem. Chem. Phys.* **2016**, *18* (1), 414–425.
- (45) Lieber, E.; Rao, C. N. R.; Thomas, A. E.; Oftedahl, E.; Minnis, R.; Nambury, C. V. N. Infrared spectra of acid azides, carbamyl azides and other azido derivatives: Anomalous splittings of the N₃ stretching bands. *Spectrochim. Acta* **1963**, *19* (7), 1135–1144.
- (46) Wu, G.; Chen, Y.; Xu, D.-J.; Liu, J.-C.; Sun, W.; Shen, Z. Synthesis and molecular structure of a tetrameric neodymium-silsesquioxane cage complex: {[(-C₄H₉)₇(Si₇O₁₂)Nd]₄NaCl}. *J. Organomet. Chem.* **2009**, *694* (9), 1571–1574.
- (47) Igonin, V. A.; Lindeman, S. V.; Struchkov, Y. T.; Molodtsova, Y. A.; Pozdnyakova, Y. A.; Shchegolikhina, O. I.; Zhdanov, A. A. Crystal structure of the Nd, Gd, and Dy sandwich complexes involving 8-membered macrocyclic phenylsiloxanolate ligands. *Russ. Chem. Bull.* **1993**, *42* (1), 176–181.
- (48) Wang, R.; Liu, H.; Carducci, M. D.; Jin, T.; Zheng, C.; Zheng, Z. Lanthanide Coordination with α -Amino Acids under Near Physiological pH Conditions: Polymetallic Complexes Containing the Cubane-Like [Ln₄(μ_3 -OH)₄]⁸⁺ Cluster Core. *Inorg. Chem.* **2001**, *40* (12), 2743–2750.
- (49) Shannon, R. D. Revised effective ionic radii and systematic studies of interatomic distances in halides and chalcogenides. *Acta Crystallogr., Sect. A: Cryst. Phys., Diffr., Theor. Gen. Crystallogr.* **1976**, *32* (5), 751–767.
- (50) Neufeld, R.; Stalke, D. Accurate molecular weight determination of small molecules via DOSY-NMR by using external calibration curves with normalized diffusion coefficients. *Chem. Sci.* **2015**, *6* (6), 3354–3364.
- (51) Bachmann, S.; Neufeld, R.; Dzemska, M.; Stalke, D. New External Calibration Curves (ECCs) for the Estimation of Molecular Weights in Various Common NMR Solvents. *Chem. - Eur. J.* **2016**, *22* (25), 8462–8465.
- (52) Bachmann, S.; Gernert, B.; Stalke, D. Solution structures of alkali metal cyclopentadienides in THF estimated by ECC-DOSY NMR-spectroscopy (incl. software). *Chem. Commun.* **2016**, *52* (87), 12861–12864.

(53) Kreyenschmidt, A.-K.; Bachmann, S.; Niklas, T.; Stalke, D. Molecular Weight Estimation of Molecules Incorporating Heavier Elements from van-der-Waals Corrected ECC-DOSY. *ChemistrySelect* **2017**, *2* (24), 6957–6960.

(54) Neufeld, R.; John, M.; Stalke, D. The Donor-Base-Free Aggregation of Lithium Diisopropyl Amide in Hydrocarbons Revealed by a DOSY Method. *Angew. Chem., Int. Ed.* **2015**, *54* (24), 6994–6998.

(55) Koehne, I.; Bachmann, S.; Niklas, T.; Herbst-Irmer, R.; Stalke, D. A Novel Bulky Heteroaromatic-Substituted Methanide Mimicking NacNac: Bis(4,6-*tert*-butylbenzoxazol-2-yl)methanide in *s*-Block Metal Coordination. *Chem. - Eur. J.* **2017**, *23* (53), 13141–13149.

(56) Zhang, Q.; Yang, X.; Deng, R.; Zhou, L.; Yu, Y.; Li, Y. Synthesis and Near Infrared Luminescence Properties of a Series of Lanthanide Complexes with POSS Modified Ligands. *Molecules* **2019**, *24* (7), 1253.

(57) Le Natur, F.; Calvez, G.; Guégan, J.-P.; Le Pollès, L.; Trivelli, X.; Bernot, K.; Daigebonne, C.; Neaime, C.; Costuas, K.; Grasset, F.; Guillou, O. Characterization and Luminescence Properties of Lanthanide-Based Polynuclear Complexes Nanoaggregates. *Inorg. Chem.* **2015**, *54* (12), 6043–6054.

(58) Mazdiyasi, K. S.; Lynch, C. T.; Smith, J. S. The Preparation and Some Properties of Yttrium, Dysprosium, and Ytterbium Alkoxides. *Inorg. Chem.* **1966**, *5* (3), 342–346.

(59) Fulmer, G. R.; Miller, A. J. M.; Sherden, N. H.; Gottlieb, H. E.; Nudelman, A.; Stoltz, B. M.; Bercaw, J. E.; Goldberg, K. I. NMR Chemical Shifts of Trace Impurities: Common Laboratory Solvents, Organics, and Gases in Deuterated Solvents Relevant to the Organometallic Chemist. *Organometallics* **2010**, *29* (9), 2176–2179.

(60) Wu, D. H.; Chen, A. D.; Johnson, C. S. An improved diffusion-ordered spectroscopy experiment incorporating bipolar-gradient pulses. *J. Magn. Reson., Ser. A* **1995**, *115* (2), 260–264.

(61) Sheldrick, G. M. SHELXT - integrated space-group and crystal-structure determination. *Acta Crystallogr., Sect. A: Found. Adv.* **2015**, *71*, 3–8.

(62) Sheldrick, G. Crystal structure refinement with SHELXL. *Acta Crystallogr., Sect. C: Struct. Chem.* **2015**, *71* (1), 3–8.

(63) Hübschle, C. B.; Dittrich, B. MoleCoolQt - a molecule viewer for charge-density research. *J. Appl. Crystallogr.* **2011**, *44* (1), 238–240.

(64) Dolomanov, O. V.; Bourhis, L. J.; Gildea, R. J.; Howard, J. A. K.; Puschmann, H. OLEX2: a complete structure solution, refinement and analysis program. *J. Appl. Crystallogr.* **2009**, *42* (2), 339–341.

(65) Macrae, C. F.; Sovago, I.; Cottrell, S. J.; Galek, P. T. A.; McCabe, P.; Pidcock, E.; Platings, M.; Shields, G. P.; Stevens, J. S.; Towler, M.; Wood, P. A. Mercury 4.0: from visualization to analysis, design and prediction. *J. Appl. Crystallogr.* **2020**, *53* (1), 226–235.

(66) Spek, A. Structure validation in chemical crystallography. *Acta Crystallogr., Sect. D: Biol. Crystallogr.* **2009**, *65* (2), 148–155.